Non-Linear Vibrations and Chaos in Harmonically Excited Rectangular Plates with One-to-One Internal Resonance

S. I. CHANG, A. K. BAJAJ, and C. M. KROUSGRILL
School of Mechanical Engineering, Purdue University, West Lafayette, IN 47907, U.S.A.

(Received: 4 November 1991; accepted: 2 June 1992)

Abstract. Nonlinear flexural vibrations of a rectangular plate with uniform stretching are studied for the case when it is harmonically excited with forces acting normal to the midplane of the plate. The physical phenomena of interest here arise when the plate has two distinct linear modes of vibration with nearly the same natural frequency. It is shown that, depending on the spatial distribution of the external forces, the plate can undergo harmonic motions either in one of the two individual modes or in a mixed-mode. Stable single-mode and mixed-mode solutions can also coexist over a wide range in the amplitudes and frequency of excitation. For low damping levels, the presence of Hopf bifurcations in the mixed-mode response leads to complicated amplitude-modulated dynamics including period doubling bifurcations, chaos, coexistence of multiple chaotic motions, and crisis, whereby the chaotic attractors suddenly disappear and the plate resumes small amplitude harmonic motions in a single-mode. Numerical results are presented specifically for 1 : 1 resonance in the (1, 2) and (3, 1) plate modes.

Key words: Coupled mode dynamics, primary resonance, chaotic motions, bifurcations.

1. Introduction

Nonlinear motions of thin elastic plates have been investigated for free vibrations, forced vibrations with forces normal to the midplane as well as parametrically excited motions with forces in the plane of the plate. A review of the literature can be found in Nayfeh and Mook [1] and Sathyamoorthy [2, 3].

In recent years, many studies [4–7] have appeared on the multi-degree-of-freedom systems where internal resonance gives rise to coupling between the modal responses and results in amplitude-modulated as well as chaotic motions, even under harmonic excitation. Such responses can also arise in continuous structural systems, specially when the structural members satisfy certain symmetry requirements. For example, in square plates, antisymmetric modes appear in pairs with one linear natural frequency of oscillation. Among the studies in continuous systems accounting for internal resonance, and thus involving more than one mode, are the works of Sridhar *et al.* [8], Maewal [9], Yasuda and Torii [10], Johnson and Bajaj [11], and Yang and Sethna [12].

In the present work, the dynamic response of a rectangular plate to harmonic excitations is investigated. It is known that for appropriate aspect ratios, the plate has two or more modes with identical frequencies. The analysis here is a generalization of the study of Yasuda and Asano [13] who studied the response of a rectangular membrane. The von Karman plate equations, accounting for membrane forces, are first reduced via the Galerkin procedure, to two second-order nonlinear modal equations. The method of averaging [1, 14] is then utilized to transform the

Nonlinear Dynamics **4**: 433–460, 1993.

modal equations to four first-order differential equations representing the slow-time evolution of amplitudes of harmonic motion of the two modes. These amplitude or averaged equations are a generalization of those that describe the motion of square plates [12] and membranes [10] and, when the additional restriction of circular symmetry is imposed, they have arisen in the study of resonant motions of a spherical pendulum [4], a stretched string [11], and forced response of axisymmetric shells [15] and beams [9]. The amplitude equations for the rectangular plate depend on three nonlinear coefficients, in contrast to the two independent nonlinear coefficients found in the above mentioned studies.

The amplitude equations are analyzed for steady-state constant solutions and their various bifurcations as the excitation frequency and amplitude, and the modal damping are varied. The motions of rectangular plates with two identical frequencies are classified depending on the nonlinear coefficients defining the plate aspect ratio and the spatial modes in resonance. Dynamic solutions bifurcating from constant solutions are obtained by using AUTO [16] and a direct time integration of the amplitude equations.

2. Formulation of the Problem

Consider a rectangular plate of thickness h and edge lengths a and b. Let $Oxyz$ be a Cartesian coordinate system with Oxy in the midplane of the plate and the origin at a corner. The plate is subjected to a uniform stretching force N_0. Under these conditions, the von Karman-type equations of motion for the plate are as follows:

$$\rho h w_{,tt} - N_0(w_{,xx} + w_{,yy}) + D(w_{,xxxx} + 2w_{,xxyy} + w_{,yyyy}) = F_{,yy}w_{,xx} - 2F_{,xy}w_{,xy} + F_{,xx}w_{,yy} - cw_{,t} + q\,, \tag{1}$$

$$F_{,xxxx} + 2F_{,xxyy} + F_{,yyyy} = Eh(w_{,xy}^2 - w_{,xx}w_{,yy})\,, \tag{2}$$

where $w(x, y, t)$, $F(x, y, t)$ and $q(x, y, t)$ are the transverse deflection, the stress function, and the external force normal to the plate, respectively. The parameters ρ, E, D and c are the density, the Young's modulus, the bending stiffness, and the damping coefficient, respectively. Furthermore, the subscript x, y or t denotes a partial differentiation with respect to that variable. We should note here that more general plate models are now available in the literature [17]. For thin plates, however, von Karman equations are a sufficiently accurate approximation.

Introducing the following transformations for the variables and parameters in equations (1) and (2)

$$x' = \frac{x}{a}\,, \qquad y' = \frac{y}{b}\,, \qquad \kappa = \frac{a}{b}\,,$$

$$t' = \frac{\pi}{a}\sqrt{\frac{N_0}{\rho h}}\,t\,, \qquad w' = \frac{w}{h}\,,$$

$$c' = \frac{a}{\pi}\sqrt{\frac{1}{\rho h N_0}}\,c\,, \qquad q' = \frac{a^2}{\pi^2 h N_0}\,q\,,$$

$$F' = \frac{F}{Eh^3\kappa^2}, \qquad \varepsilon' = \frac{Eh^3\kappa^2}{N_0\pi^2 b^2},$$
$$D' = \frac{D}{\pi^2 N_0 a^2}, \tag{3}$$

and omitting primes, equations (1) and (2) take the following nondimensional forms:

$$w_{,tt} - \frac{1}{\pi^2}(w_{,xx} + \kappa^2 w_{,yy}) + D(w_{,xxxx} + 2\kappa^2 w_{,xxyy} + \kappa^4 w_{,yyyy})$$
$$= \varepsilon(F_{,yy}w_{,xx} - 2F_{,xy}w_{,xy} + F_{,xx}w_{,yy}) - cw_{,t} + q, \tag{4}$$

$$F_{,xxxx} + 2\kappa^2 F_{,xxyy} + \kappa^4 F_{,yyyy} = w_{,xy}^2 - w_{,xx}w_{,yy}, \tag{5}$$

where the dimensionless parameters ε, κ, D and c represent the thickness parameter, the aspect ratio, the ratio of bending stiffness to uniform stretching force and the damping coefficient, respectively.

The boundary conditions considered here are that all the edges are simply supported and immovable. The transverse displacement w then satisfies

$$w = w_{,xx} = 0 \quad \text{at} \quad x = 0, 1,$$
$$\text{and } w = w_{,yy} = 0 \quad \text{at} \quad y = 0, 1.$$

The in-plane boundary conditions of $u = v = 0$ along the four sides of the plate, where u and v are the in-plane displacements in the x and y direction, respectively, can be satisfied only on the average [13]. These conditions put in terms of the stress function F and expressed in nondimensional form, are as follows:

$$\int_0^1 \int_0^1 \left(\kappa^4 F_{,yy} - \nu\kappa^2 F_{,xx} - \frac{1}{2}w_{,x}^2\right) dx\, dy = 0,$$
$$\int_0^1 \int_0^1 \left(F_{,xx} - \nu\kappa^2 F_{,yy} - \frac{1}{2}w_{,y}^2\right) dx\, dy = 0,$$
$$\int_0^1 \int_0^1 (2(1+\nu)\kappa^2 F_{,xy} + w_{,x}w_{,y})\, dx\, dy = 0, \tag{6}$$

where ν is the Poisson's ratio.

The interest in the present study is in motions when the plate is harmonically excited by the external force $q(x, y, t)$. Large amplitude motions occur when the excitation frequency is near a linear natural frequency and the motions of the plate are approximated by the linear vibratory modes. Employing the Galerkin method, equations (4)–(5) can be transformed into a set of nonlinear ordinary differential equations governing the modal amplitudes of response for the plate.

The plate deflection function w can, in general, be chosen as

$$w(x, y, t) = \sum X_i(t)\phi_i(x, y) \tag{7}$$

where $\phi_i(x, y)$ are a set of comparison functions. In this study, we assume the deflection to be a superposition of two distinct linear modes as follows:

$$w(x, y, t) = X_1(t) \sin m\pi x \sin n\pi y + X_2(t) \sin r\pi x \sin s\pi y \,. \tag{8}$$

Thus, the motion consists of a linear combination of the two spatial modes of orders (m, n) and (r, s). The modal amplitudes X_1 and X_2 are functions of time and the nonlinear terms in the system determine their time evolution. Substituting equation (8) into equation (5), the solution for the resulting linear partial differential equation in the stress function F can be written as

$$F(x, y, t) = F^h(x, y, t) + F^p(x, y, t) \,, \tag{9}$$

where F^h is the homogeneous solution which includes the effect of the in-plane stretching forces independent of the transverse deflection, and F^p is the particular solution that includes the effect of out-of-plane boundary conditions. The particular solution F^p can be easily shown to be [13]

$$\begin{aligned} F^p(x, y, t) = {} & \frac{1}{32}\left(\frac{n^2}{m^2}\cos 2m\pi x + \frac{m^2}{n^2\kappa^4}\cos 2n\pi y\right) X_1^2 \\ & + \frac{1}{32}\left(\frac{s^2}{r^2}\cos 2r\pi x + \frac{r^2}{s^2\kappa^4}\cos 2s\pi y\right) X_2^2 \\ & + \frac{1}{4}\left[-\frac{(ms - nr)^2}{\{(m+r)^2 + \kappa^2(n+s)^2\}^2}\cos (m+r)\pi x \cos (n+s)\pi y \right. \\ & + \frac{(ms + nr)^2}{\{(m+r)^2 + \kappa^2(n-s)^2\}^2}\cos (m+r)\pi x \cos (n-s)\pi y \\ & + \frac{(ms + nr)^2}{\{(m-r)^2 + \kappa^2(n+s)^2\}^2}\cos (m-r)\pi x \cos (n+s)\pi y \\ & \left. + \frac{-(ms - nr)^2}{\{(m-r)^2 + \kappa^2(n-s)^2\}^2}\cos (m-r)\pi x \cos (n-s)\pi y \right] X_1 X_2 \,. \end{aligned} \tag{10}$$

For F^h to satisfy the boundary conditions, equations (6), the homogeneous solution F^h can be assumed as

$$F^h(x, y, t) = \frac{1}{2} N_{x0} y^2 + \frac{1}{2} N_{y0} x^2 + N_{xy0} xy \,. \tag{11}$$

Substituting $F = F^p + F^h$ into the in-plane boundary conditions, equations (6), and carrying though the algebra, the time dependent functions N_{x0}, N_{y0}, and N_{xy0} turn out to be

$$\begin{aligned} N_{x0} &= \frac{\pi^2}{8(1-\nu^2)\kappa^4}\left[(m^2X_1^2 + r^2X_2^2) + \nu\kappa^2(n^2X_1^2 + s^2X_2^2)\right] , \\ N_{y0} &= \frac{\pi^2}{8(1-\nu^2)\kappa^4}\left[\kappa^4(n^2X_1^2 + s^2X_2^2) + \nu\kappa^2(m^2X_1^2 + r^2X_2^2)\right] , \end{aligned} \tag{12}$$

and

$$N_{xy0} = 0 \,.$$

N_{xy0} is nonzero only when both $(m \pm r)$ and $(n \pm s)$ are odd numbers and its expression is given in [13]. Substituting the solution F obtained above and the assumed two mode solution, equation (8), into equation (4), multiplying successively, by $\sin m\pi x \sin n\pi y$ and $\sin r\pi x \sin s\pi y$, and integrating over the domain of the plate, we get the following discretized equations of motion:

$$\ddot{X}_1 + p_1^2 X_1 = \varepsilon N_1(X_1, X_2) - c\dot{X}_1 + q_1 ,$$
$$\ddot{X}_2 + p_2^2 X_2 = \varepsilon N_2(X_1, X_2) - c\dot{X}_2 + q_2 , \tag{13}$$

where εN_1 and εN_2 are nonlinear functions of order 3 in X_1 and X_2,

$$p_1^2 = p_{mm}^2 = (m^2 + \kappa^2 n^2) + D\pi^4 (m^2 + \kappa^2 n^2)^2 ,$$
$$p_2^2 = p_{rs}^2 = (r^2 + \kappa^2 s^2) + D\pi^4 (r^2 + \kappa^2 s^2)^2 , \tag{14}$$

$$q_1 = 4 \int_0^1 \int_0^1 q(x, y, t) \sin m\pi x \sin n\pi y \, dx \, dy ,$$

and

$$q_2 = 4 \int_0^1 \int_0^1 q(x, y, t) \sin r\pi x \sin s\pi y \, dx \, dy . \tag{15}$$

Here p_1 and p_2 are the nondimensional natural frequencies for the two linear (m, n) and (r, s) modes of the plate, and q_1 and q_2 are the contributions of the transverse excitation q to the two modes. If the external force q is expanded as

$$q(x, y, t) = \sum_{i,j} q_{ij}(t) \sin i\pi x \sin j\pi y , \tag{16}$$

equation (15) gives

$$q_1 = q_{mn}(t) ,$$
$$q_2 = q_{rs}(t) . \tag{17}$$

Using equations (14), it can be easily shown that there exist various combinations of two specific linear modes and the corresponding values of the aspect ratio κ which result in degeneracy of modes, that is, for some specific value of κ, two different spatial modes have the same natural frequency. The results for lower mode numbers (i, j), $1 \le i, j \le 5$ are shown in Figure 1. Using equations (14) it is easy to show that the values of κ at which the degeneracy of two specific modes arise are independent of the bending stiffness D of the plate. Thus, for a particular mode combination determined by (m, n) and (r, s), the two linear natural frequencies are equal at a specific aspect ratio κ. Clearly, there are many aspect ratios κ at which multiple eigenmodes arise. The likelihood of more than one set of multiple eigenmodes arising at the same aspect ratio increases with the mode numbers. In the present work we assume that only two linear natural frequencies are coincident and that no other internal or combination resonances arise. The numerical values of natural frequencies do depend on the bending stiffness D. For specific numerical results we have selected the two interacting modes to be the $(1, 2)$ and $(3, 1)$ plate modes. The analysis, however, is completely general and applies to all the cases with two modes in

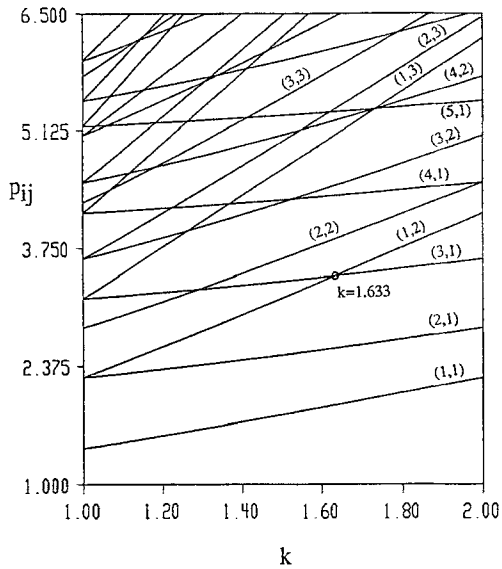

Fig. 1. Dependence of linear natural frequencies for the various plate modes on the aspect ratio κ.

1 : 1 internal resonance. Their natural frequencies are identical when the aspect ratio κ is 1.633. The excitation force is assumed to be harmonic so that q_1 and q_2 in equations (17) are given by

$$q_i = Q_i \cos \omega t\,, \qquad i = 1, 2\,. \tag{18}$$

Under these conditions equations (13) become

$$\begin{aligned} &\ddot{X}_1 + p_1^2 X_1 = \varepsilon(A_1 X_1^2 + A_2 X_2^2) X_1 - c\dot{X}_1 + Q_1 \cos \omega t\,, \\ &\ddot{X}_2 + p_2^2 X_2 = \varepsilon(A_2 X_1^2 + A_3 X_2^2) X_2 - c\dot{X}_2 + Q_2 \cos \omega t\,, \end{aligned} \tag{19}$$

where A_1, A_2 and A_3 are the constant non-linear coefficients which are determined for the specific mode combinations, and p_1 and p_2 are the corresponding natural frequencies of the two linear modes. The expressions for A_1, A_2 and A_3, in terms of the mode numbers (m, n) and (r, s) and the aspect ratio κ, are given in the Appendix.

Let

$$\begin{aligned} X_1 &= R_1 \cos(\omega t - \gamma_1)\,, \\ X_2 &= R_2 \cos(\omega t - \gamma_2)\,. \end{aligned} \tag{20}$$

Then, using a variation of constants procedure and the method of averaging [1, 14, 18], and noting that the excitation frequency ω is near the two close natural frequencies, equations (19) result in the following averaged equations for the amplitudes R_i and the phases γ_i:

$$\begin{aligned} \dot{R}_1 &= -\frac{c}{2} R_1 + \frac{Q_1}{2\omega} \sin \gamma_1 + \frac{\varepsilon A_2}{8\omega} R_2^2 R_1 \sin 2(\gamma_1 - \gamma_2)\,, \\ \dot{\gamma}_1 &= \frac{\omega^2 - p_1^2}{2\omega} + \frac{Q_1}{2\omega R_1} \cos \gamma_1 + \frac{3\varepsilon A_1}{8\omega} R_1^2 + \frac{\varepsilon A_2}{8\omega} R_2^2 \{2 + \cos 2(\gamma_1 - \gamma_2)\}\,, \end{aligned}$$

$$\dot{R}_2 = -\frac{c}{2} R_2 + \frac{Q_2}{2\omega} \sin \gamma_2 + \frac{\varepsilon A_2}{8\omega} R_1^2 R_2 \sin 2(\gamma_2 - \gamma_1) ,$$

$$\dot{\gamma}_2 = \frac{\omega^2 - p_2^2}{2\omega} + \frac{Q_2}{2\omega R_2} \cos \gamma_2 + \frac{3\varepsilon A_3}{8\omega} R_2^2 + \frac{\varepsilon A_2}{8\omega} R_1^2 \{2 + \cos 2(\gamma_2 - \gamma_1)\} . \tag{21}$$

These equations were also derived and studied by Yasuda and Asano in [13] for the case of a rectangular membrane. Given a specific value of the aspect ratio κ, and the degeneracy of two specific modes, the plate and the membrane have the same averaged or amplitude equations. The nonlinear coefficients A_1, A_2 and A_3 depend only on the mode combinations, the Poison's ratio, and the form of the nonlinearity assumed (von Karman-type nonlinearities). The values of the natural frequencies p_1 and p_2 are however different.

We should note that the procedure used here in deriving the averaged equations is along the lines of [13] although it can be easily formalized by introducing a small parameter and by scaling the modal amplitudes X_i, $i = 1, 2$, the damping c, and the external force amplitudes Q_i, $i = 1, 2$, appropriately (e.g., see Nayfeh and Mook [1] and Johnson and Bajaj [11]). The resulting amplitude equations will be identical to equations (21), except for the small parameter multiplying the right hand side. Thus, the amplitude equations should be treated in the sense of a slow time scale. Also note that $p_1^2 \approx p_2^2 \approx \omega^2$, and thus, the problem under study is an example of primary resonant motions in systems of coupled oscillators with 1 : 1 internal resonance and cubic nonlinearities [1].

In a general external loading case, the force amplitudes Q_1 and Q_2 are not zero. There can be special situations when one (both) of them is (are) zero depending on the spatial distribution of the loading and the mode numbers in internal resonance. Yasuda and Asano [13] presented results for $Q_1 = Q_2 = 10.0$. Here, we are much more interested in the situation when only one mode is externally excited and the second mode is driven due to its nonlinear coupling to the excited mode. Two such specific cases arise, i.e., $Q_1 \neq 0$ and $Q_2 = 0$, or $Q_1 = 0$ and $Q_2 \neq 0$. Due to the similar nature of the equations for (R_1, γ_1) and for (R_2, γ_2), the analytical expressions for various steady-state constant solutions turn out to be identical except for the role of the nonlinear coefficients A_1 and A_3. In view of the possible bifurcations and stability considerations, however, considerable qualitative as well as quantitative differences in the overall response can arise in the two cases. We describe these in the next section where a local bifurcation analysis of equations (21) is carried out. In fact, it is shown that the qualitative behavior is strongly dependent on the nonlinear coefficients, and rectangular plates with two interacting modes in 1 : 1 resonance can be classified based on the nonlinear coefficients.

Finally, it is easy to see that the divergence of the averaged system (21), when expressed in Cartesian form (equations (28)),

$$\sum_{i=1}^{2} \left(\frac{\partial \dot{u}_i}{\partial u_i} + \frac{\partial \dot{v}_i}{\partial v_i} \right) ,$$

is $-2c$ from which it follows that the volume in (u_1, v_1, u_2, v_2) space contracts and that every solution trajectory must ultimately be confined to a limiting subspace of dimension less than four. Furthermore, equations (21) can be combined to show that

$$\frac{\mathrm{d}E}{\mathrm{d}t} = -\frac{c}{2} E + \frac{Q_1}{2\omega} \left(\frac{R_1 \sin \gamma_1}{E} \right) + \frac{Q_2}{2\omega} \left(\frac{R_2 \sin \gamma_2}{E} \right) ,$$

where $E^2 = R_1^2 + R_2^2$. This has the implicit solution

$$E(t) = E(0)e^{-(c/2)t} + \int_0^t \left[\frac{Q_1}{2\omega}\left(\frac{R_1 \sin \gamma_1}{E}\right) + \frac{Q_2}{2\omega}\left(\frac{R_2 \sin \gamma_2}{E}\right)\right] e^{-\frac{c}{2}(t-\tau)}\, d\tau .$$

Noting that $|R_i \sin \gamma_i / E| \leq 1$, $i = 1, 2$, we get the inequality

$$|E(t) - E(0)e^{-\frac{c}{2}t}| \leq \frac{1}{c\omega}\left(1 - e^{-\frac{c}{2}t}\right)(Q_1 + Q_2) .$$

Thus, the steady-state solution is ultimately ($t \to \infty$) bounded and confined to a hypersphere of radius $(Q_1 + Q_2)/c\omega$.

3. Steady-State Solutions and Bifurcation Analysis

3.1. Steady-State Solutions

As already discussed, we emphasize the cases when only one of the two modes is externally excited. First, consider the case when $Q_2 = 0$ and $Q_1 \neq 0$. Thus, the (m, n) mode is directly excited by an external harmonic force. There are two types of steady-state constant solutions. One set of solutions is characterized by the fact that $R_2 = 0$, that is, the indirectly excited mode is absent. Then the only response is in the (m, n) mode with $R_1 \neq 0$ and this is called the single-mode solution. The other class of solutions corresponds to both R_1 and R_2 being nonzero and such motions are called the coupled-mode response. A similar situation exists when the (r, s) mode is directly excited and $Q_1 = 0$.

From equations (21), the steady-state constant solutions for single-mode motions are determined by

$$\begin{aligned}
&\frac{c}{2}\bar{R}_1 - \frac{Q_1}{2\omega}\sin \bar{\gamma}_1 = 0 ,\\
&\frac{\omega^2 - p_1^2}{2\omega}\bar{R}_1 + \frac{3\varepsilon A_1}{8\omega}\bar{R}_1^3 + \frac{Q_1}{2\omega}\cos \bar{\gamma}_1 = 0 ,\\
&\bar{R}_2 = 0 ,
\end{aligned} \tag{22}$$

where an overbar indicates the single-mode steady-state solutions. Combining the equations for R_1 and γ_1 results in the following polynomial in $\bar{R}_1$:

$$\bar{R}_1^6 + \frac{8(\omega^2 - p_1^2)}{3\varepsilon A_1}\bar{R}_1^4 + \frac{16[\omega^2 c^2 + (\omega^2 - p_1^2)^2]}{9\varepsilon^2 A_1^2}\bar{R}_1^2 - \frac{16Q_1^2}{9\varepsilon^2 A_1^2} = 0 . \tag{23}$$

Real roots of equation (23) determine the single-mode steady-state constant solutions. Note that equations (22), or equivalently the polynomial (23), are identical to those arising in the primary resonant response of the harmonically excited Duffing equation [1].

Differentiating equation (23) with respect to $\bar{R}_1$ and setting $\partial\omega/\partial\bar{R}_1 = 0$ gives, the saddle-node bifurcation points [18] or, the points of vertical tangency for single-mode steady-state solutions:

$$(\bar{R}_1^2)_{SNS} = \frac{4}{9\varepsilon A_1}\left[-2(\omega^2 - p_1^2) \pm \sqrt{(\omega^2 - p_1^2)^2 - 3c^2\omega^2}\right]. \tag{24}$$

Here the subscript SNS implies the saddle-node bifurcation for single-mode solutions. We will show later that equation (24) also corresponds to the occurrence of zero eigenvalues when the stability of solutions in the single-mode branches is considered.

The problem of finding steady-state constant solutions for coupled-mode response ($R_1 \neq 0$, $R_2 \neq 0$) can also be formulated as that of finding the real roots of a polynomial of the 8th order in $\hat{R}_2^2$, where a hat indicates the coupled-mode steady-state solution. Due to its complexity, the polynomial expression in R_2 has been determined by using symbolic algebra programs (e.g., SMP, MACSYMA) and is not presented here. The corresponding expression for the coupled-mode steady-state solution $\hat{R}_1$ is given by

$$\hat{R}_1^2 = -2\left[\frac{A_3}{A_2}\hat{R}_2^2 + \frac{4}{3}\frac{(\omega^2 - p_2^2)}{\varepsilon A_2}\right] \pm \sqrt{\left[\frac{A_3}{A_2}\hat{R}_2^2 + \frac{4}{3}\frac{(\omega^2 - p_2^2)}{\varepsilon A_2}\right]^2 - \frac{16}{3}\frac{\omega^2 c^2}{\varepsilon^2 A_2^2}}. \tag{25}$$

When damping is absent, the equation governing the amplitude $\hat{R}_2$ is of the form

$$C_1\hat{R}_2^8 + C_2\hat{R}_2^6 + C_3\hat{R}_2^4 + C_4\hat{R}_2^2 + C_5 = 0,$$

where the coefficients of the polynomial are a function of the parameters A_1, A_2, A_3, ω, p_1, p_2, ε and Q_1. The expressions for coefficients C_i, $i = 1, 2, 3, 4, 5$, are given in the Appendix.

Setting $\hat{R}_2 = 0$ in equation (25), we can obtain the critical points for the onset of coupled-mode steady-state harmonic response. The condition for the occurrence of pitchfork bifurcation from the single-mode response is

$$(\hat{R}_1^2)_{PF} = \frac{4}{3\varepsilon A_2}\left[-2(\omega^2 - p_2^2) \pm \sqrt{(\omega^2 - p_2^2)^2 - 3c^2\omega^2}\right], \tag{26}$$

where PF refers to a pitchfork bifurcation [18]. We will show later that equation (26) also corresponds to the occurrence of a zero eigenvalue.

It is clear from the polynomials (23) and (25) that, given the mode numbers (m, n) and (r, s), and the aspect ratio κ, the number of real solutions of the single-mode and the coupled-mode type depends on the physical parameters p_1, p_2, c, ω, and Q_1. While the condition of $\kappa = 1.633$ fixes the two natural frequencies $p_1 = p_2$, any small deviations from the precise value of the aspect ratio lead to small mistuning in the internally resonant modes and thus $(p_1^2 - p_2^2)$ is an important "internal" mistuning parameter. The other frequency parameter is $(\omega^2 - p_1^2)$ or $(\omega^2 - p_2^2)$ which represents the "external" mistuning. Numerical values of the natural frequencies p_1 and p_2, as indicated earlier, depend also on the bending stiffness D and the Poisson's ratio ν. The nonlinear coefficients A_1, A_2, and A_3, however, depend only on the Poisson's ratio.

Figure 2 shows the various single-mode and coupled-mode steady-state constant solutions R_1 and R_2 as a function of the excitation frequency ω. These response curves are for (1, 2) and (3, 1) interacting modes with the damping $c = 0.0$, and force amplitudes $Q_1 = 10.0$ and $Q_2 = 0.0$. For all the numerical results presented in this work $\varepsilon = 6 \times 10^{-4}$, $\nu = 0.3$, $p_1^2 = p_2^2 = 35/3$, and $D = 0.0$. The nonlinear coefficients for the (1, 2) and (3, 1) modes are $A_1 = -326.27$, $A_2 = -274.79$ and $A_3 = -268.32$. The frequency axis is divided into 4 intervals, I, II, III, and IV, according to the nature of solutions. Over the interval I, there exists only one single-mode solution. Over the

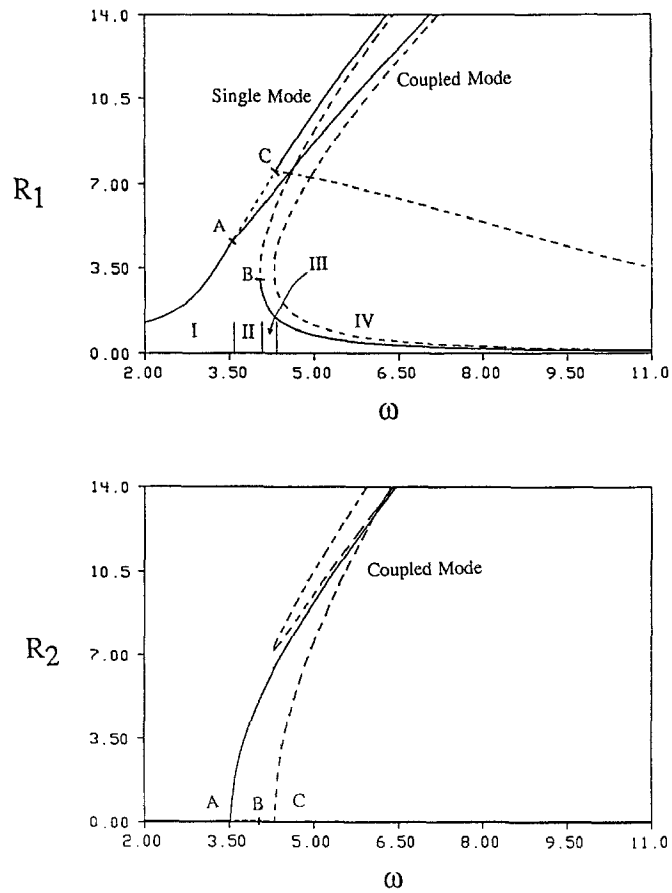

Fig. 2. Constant amplitude response R_1, for the (1, 2) plate mode, and R_2, for the (3, 1) plate mode, as a function of the excitation frequency ω; $Q_1 = 10.0$, $Q_2 = 0.0$, $c = 0.0$.

interval II, we have a stable coupled-mode solution and an unstable single-mode solution. Therefore, in the intervals I and II, the initial condition is not critical to determining the final steady-state response. Over the frequency intervals III and IV, there exist a stable single-mode and a stable coupled-mode solution, and two stable single-mode and a stable coupled-mode solutions, respectively. Thus, the initial condition is very important in determining the final steady-state response reached in any experiment or numerical simulation. Note also that for every mixed-mode solution with some γ_2, there is another solution with phase angle $\gamma_2 + \pi$ for the amplitude R_2. Thus, the response curve really represent two coupled-mode solutions which are phase shifted by π radians.

The points A and C in Figure 2 are associated with equation (26), that is, the pitchfork bifurcation points, and the point B is associated with equation (24), that is, a saddle-node bifurcation point for single-mode solution. The corresponding frequencies at the points A, B, and C coincide with the boundaries of the intervals.

The single-mode and the coupled-mode harmonic motions of the plate can also be interpreted in terms of standing and rotating nodal patterns. Clearly, for the single-mode response, the nodal

lines are stationary and the plate vibrates harmonically in the (1, 2) mode. When both (1, 2) and (3, 1) modes are present in the response, the nodal pattern depends on the phases γ_1 and γ_2. Only in the case of $\gamma_1 = \gamma_2$ or $\gamma_1 = \gamma_2 \pm \pi$ are the nodal patterns stationary. Otherwise, the nodal pattern changes continuously in a periodic manner, resulting in a traveling wave motion of the plate.

A similar analysis can be performed for the case when $Q_1 = 0$ and $Q_2 \neq 0$. Figure 3 shows the response curves for this case with $Q_1 = 0$ and $Q_2 = 10.0$. From the figure, it is seen that over the intervals I, II, and III, we have qualitatively the same results. Over the interval IV, however, there exist one stable single-mode and one stable coupled-mode solution in this case, whereas, there are two stable single-mode solutions and one stable coupled-mode solution for the case with $Q_1 = 10.0$ and $Q_2 = 0$. This qualitative difference arises due to the fact that here one of the pitchfork bifurcations from the single-mode solutions occurs in the lower branch (point C) while in the earlier case both the pitchfork bifurcations occur only in the upper branch of the single-mode solutions. As is shown in Section 4, this is a consequence of the relative magnitude of the nonlinear coefficients A_i, $i = 1, 2, 3$. Further discussion about other qualitative differences between the responses for the two cases will be given following the stability analysis.

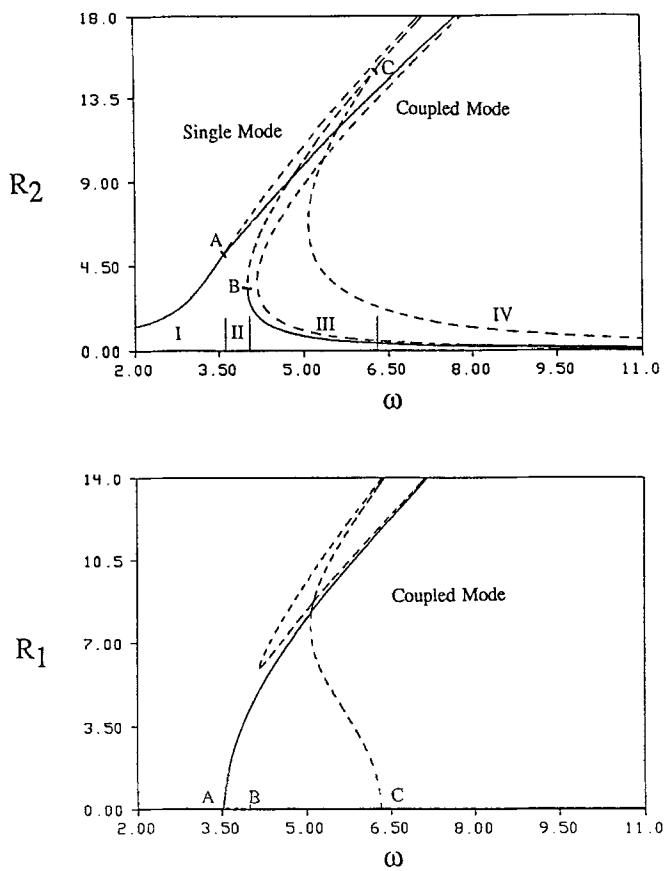

Fig. 3. Constant amplitude response R_1, for the (1, 2) plate mode, and R_2, for the (3, 1) plate mode, as a function of the excitation frequency ω; $Q_1 = 0.0$, $Q_2 = 10.0$, $c = 0.0$.

3.2. *Stability Analysis*

Stability analysis of steady-state constant solutions of the averaged equations is most readily accomplished with equations in Cartesian form. Letting

$$u_i = R_i \cos \gamma_i , \qquad v_i = R_i \sin \gamma_i , \qquad i = 1, 2 , \tag{27}$$

the transformed averaged equations in Cartesian variables (u_i, v_i), $= 1, 2$, are given by

$$\begin{aligned}
\dot{u}_1 &= -\frac{c}{2} u_1 - \frac{\omega^2 - p_1^2}{2\omega} v_1 - \frac{3\varepsilon A_1}{8\omega} v_1 (u_1^2 + v_1^2) + \frac{\varepsilon A_2}{8\omega} (-v_1 u_2^2 - 3v_1 v_2^2 - 2u_1 u_2 v_2) , \\
\dot{v}_1 &= -\frac{c}{2} v_1 + \frac{Q_1}{2\omega} + \frac{\omega^2 - p_1^2}{2\omega} u_1 + \frac{3\varepsilon A_1}{8\omega} u_1 (u_1^2 + v_1^2) + \frac{\varepsilon A_2}{8\omega} (3u_1 u_2^2 + u_1 v_2^2 + 2v_1 u_2 v_2) , \\
\dot{u}_2 &= -\frac{c}{2} u_2 - \frac{\omega^2 - p_2^2}{2\omega} v_2 - \frac{3\varepsilon A_3}{8\omega} v_2 (u_2^2 + v_2^2) + \frac{\varepsilon A_2}{8\omega} (-v_2 u_1^2 - 3v_2 v_1^2 - 2u_2 u_1 v_1) , \\
\dot{v}_2 &= -\frac{c}{2} v_2 + \frac{Q_2}{2\omega} + \frac{\omega^2 - p_2^2}{2\omega} u_2 + \frac{3\varepsilon A_3}{8\omega} u_2 (u_2^2 + v_2^2) + \frac{\varepsilon A_2}{8\omega} (3u_2 u_1^2 + u_2 v_1^2 + 2v_2 u_1 v_1) .
\end{aligned} \tag{28}$$

The eigenvalues of the Jacobian matrix of (28), which determine the stability of the single-mode solutions ($u_2 = v_2 = 0$, or $R_2 = 0$) with $Q_2 = 0$, can be shown to satisfy the two quadratics:

$$\lambda^2 + c\lambda + \frac{1}{2}\left[c^2 + \frac{27\varepsilon^2 A_1^2}{16\omega^2} \bar{R}_1^4 + \frac{3\varepsilon A_1 (\omega^2 - p_1^2)}{\omega^2} \bar{R}_1^2 + \frac{(\omega^2 - p_1^2)^2}{\omega^2} \right] = 0 , \tag{29a}$$

$$\lambda^2 + c\lambda + \frac{1}{2}\left[c^2 + \frac{3\varepsilon^2 A_2^2}{16\omega^2} \bar{R}_1^4 + \frac{\varepsilon A_2 (\omega^2 - p_2^2)}{\omega^2} \bar{R}_1^2 + \frac{(\omega^2 - p_2^2)^2}{\omega^2} \right] = 0 , \tag{29b}$$

where λ represents the eigenvalue. Using equations (29) and the fact that $\bar{R}_1$ is a root of (23), it can be easily shown that no eigenvalue can be purely imaginary for $c \neq 0$ and, as a result, Hopf bifurcation [18] cannot arise from the single-mode steady-state solutions. Therefore, the single-mode steady-state solutions can lose their stability only when an eigenvalue becomes zero. Using equations (29), the conditions for the loss of stability with a zero eigenvalue turn out to be

$$c^2 + \frac{27\varepsilon^2 A_1^2}{16\omega^2} \bar{R}_1^4 + \frac{3\varepsilon A_1 (\omega^2 - p_1^2)}{\omega^2} \bar{R}_1^2 + \frac{(\omega^2 - p_1^2)^2}{\omega^2} = 0 , \tag{30a}$$

$$c^2 + \frac{3\varepsilon^2 A_2^2}{16\omega^2} \bar{R}_1^4 + \frac{\varepsilon A_2 (\omega^2 - p_2^2)}{\omega^2} \bar{R}_1^2 + \frac{(\omega^2 - p_2^2)^2}{\omega^2} = 0 . \tag{30b}$$

Equation (30a) is really equivalent to equation (24), the condition for a saddle-node bifurcation or a turning point. Similarly, equation (30b) is equivalent to equation (26), the condition for a pitchfork bifurcation. It can thus be concluded that the single-mode steady-state constant solutions lose their stability either at the saddle-node bifurcation points or at the pitchfork bifurcation points.

These saddle-node and pitchfork bifurcation sets for the single-mode solutions can be obtained in the parameter space by combining equations (23) and (30). Due to their complexities,

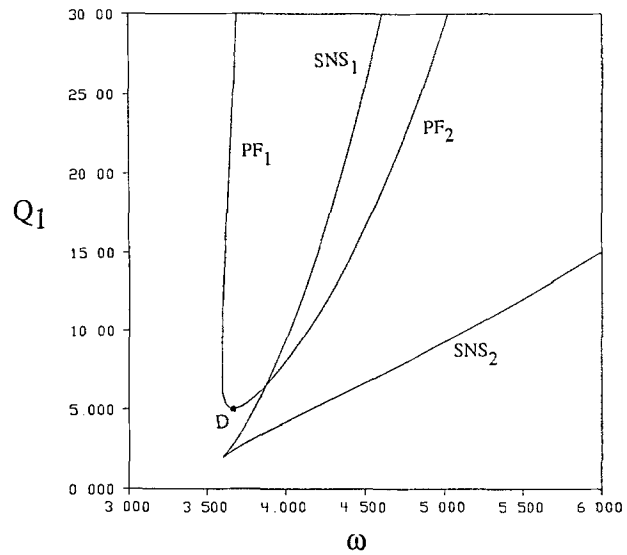

Fig. 4. Saddle-node and pitchfork bifurcation sets for the single-mode solutions; $Q_2 = 0.0$, $c = 0.195$.

the equations for the bifurcation sets are not given here. A representative set of these graphs for (1, 2) and (3, 1) modes are shown in Figure 4 for $c = 0.195$. Here, SNS and PF denote, respectively, the saddle-node and the pitchfork bifurcation sets for the single-mode solutions. Note that as the force amplitude Q_1 is increased for a fixed damping, the single-mode solution first develops multiplicity and only then pitchfork bifurcations arise. This can be also shown to be the case by a careful examination of equations (30a) and (30b).

The geometry of solutions in the phase space (u_1, v_1, u_2, v_2) is quite interesting and understanding it is essential to explaining some of the phenomena and response behavior found in the study. First note that $Q_2 = 0$ implies that the (u_1, v_1) surface, that is, $(u_2, v_2) = (0.0, 0.0)$ is an invariant of the vector field defined equivalently by equations (21) or equations (28). If initial conditions are chosen in (u_1, v_1) plane, the motion governed by solutions of equations (28) remains confined to it, that is, the dynamics of the plate is a single-mode motion. For single-mode constant solutions, the instability boundary defined by equation (30a) corresponds to disturbances restricted to the (u_1, v_1) plane. The instability condition (30b) arises only when disturbances in the (u_2, v_2) plane, that is, out of the (u_1, v_1) plane are allowed. Thus, pitchfork bifurcation from single-mode to coupled-mode constant solutions arises only because of coupled-mode disturbances.

A similar stability analysis can be carried out for the coupled-mode steady-state constant solutions though the algebra becomes unmanageable and symbolic algebra programs have been utilized. Due to the complexity, this analysis is not presented here except to note that now both zero and pure-imaginary pair of eigenvalues are possible as criterion for the loss of stability. A zero eigenvalue can lead to a saddle-node bifurcation and the associated multiple coupled-mode responses, whereas, a pure-imaginary eigenvalue leads to Hopf bifurcation and the possibility of limit cycle solutions [18] for the amplitude equations. Pitchfork bifurcations also arise in the coupled-mode branches for a zero eigenvalue but they are found to correspond only to the points where the coupled-mode solutions arise from the single-mode solutions and this set is already identified above. The saddle-node and the Hopf bifurcation sets for the coupled-mode responses were obtained using AUTO [16], are denoted SNC and HB, and are shown in Figure 5 for

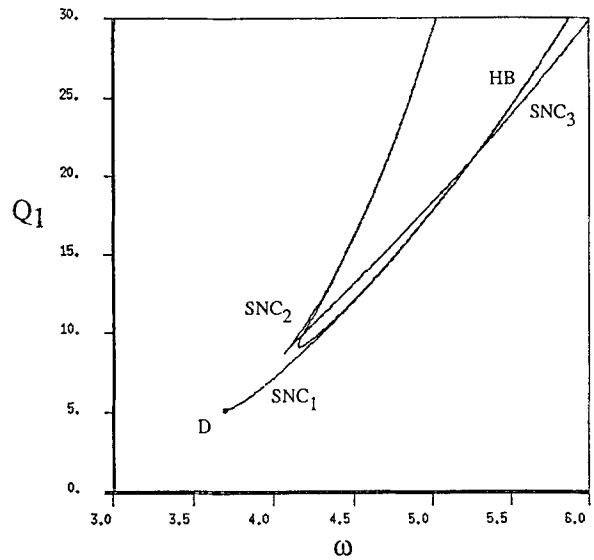

Fig. 5. Saddle-node and Hopf bifurcation sets for the coupled-mode solutions; $Q_2 = 0.0$, $c = 0.195$.

$c = 0.195$. Points at which the various bifurcation sets intersect, (see both Figures 4 and 5) have, in most cases, no special significance since the intersecting lines or curves represent instability boundaries for different solutions. The point D in Figures 4 and 5 corresponds to a double-zero eigenvalue and is therefore a codimension-2 point [18]. More complicated bifurcation phenomena are expected for values of parameters near the codimension-2 point and results of analytical investigations will be reported in a future work.

The system response depends on four parameters Q_1, ω, c and $(p_1^2 - p_2^2)$. The bifurcation sets shown in Figures 4 and 5 correspond to zero internal mistuning $(p_1^2 = p_2^2)$ and a fixed value of damping. The parameters Q_1 and c play opposite roles and, in fact, Q_1 can be eliminated by an additional scaling. It is therefore expected and seen that the bifurcation sets at other damping values are qualitatively similar to the ones shown here. Though physically more realistic, we have not yet studied in sufficient detail the case of nonzero internal mistuning.

Figures 4 and 5 show that, beginning with very small values of Q_1, as the amplitude of excitation is slowly raised, the plate response undergoes interesting and significant qualitative changes. Figures 6a–e are a series of bifurcation diagrams depicting these changes with u_1 as a function of the excitation frequency ω. For small forcing amplitudes, the response is harmonic and single-valued, that is, for each forcing frequency, the plate undergoes a unique harmonic motion in the (1, 2) mode (Figure 6a). At force levels above the cusp point on the SNS curve, the single-mode response undergoes saddle-note bifurcations and now three single-mode responses exist between the frequency boundaries SNS_1 and SNS_2 (Figure 6b). The upper and the lower solution branches are stable whereas the middle branch is unstable. Next qualitative change occurs when the pitchfork bifurcation set appears. For a very small interval in the amplitude Q_1, the pitchfork bifurcations, which occur in the upper single-mode branch, are supercritical and all the coupled-mode motions are stable. Above the codimension-2 point (point D), the pitchfork bifurcation from the right boundary, PF_2, becomes subcritical with two possible coupled-mode motions now existing between the curves PF_2 and SNC_1 (Figure 6c). The subcritical branch is unstable and saddle-type with one real positive eigenvalues. Further increase in the forcing amplitude results in two additional turning points in the coupled-mode branch, SNC_2 and SNC_3,

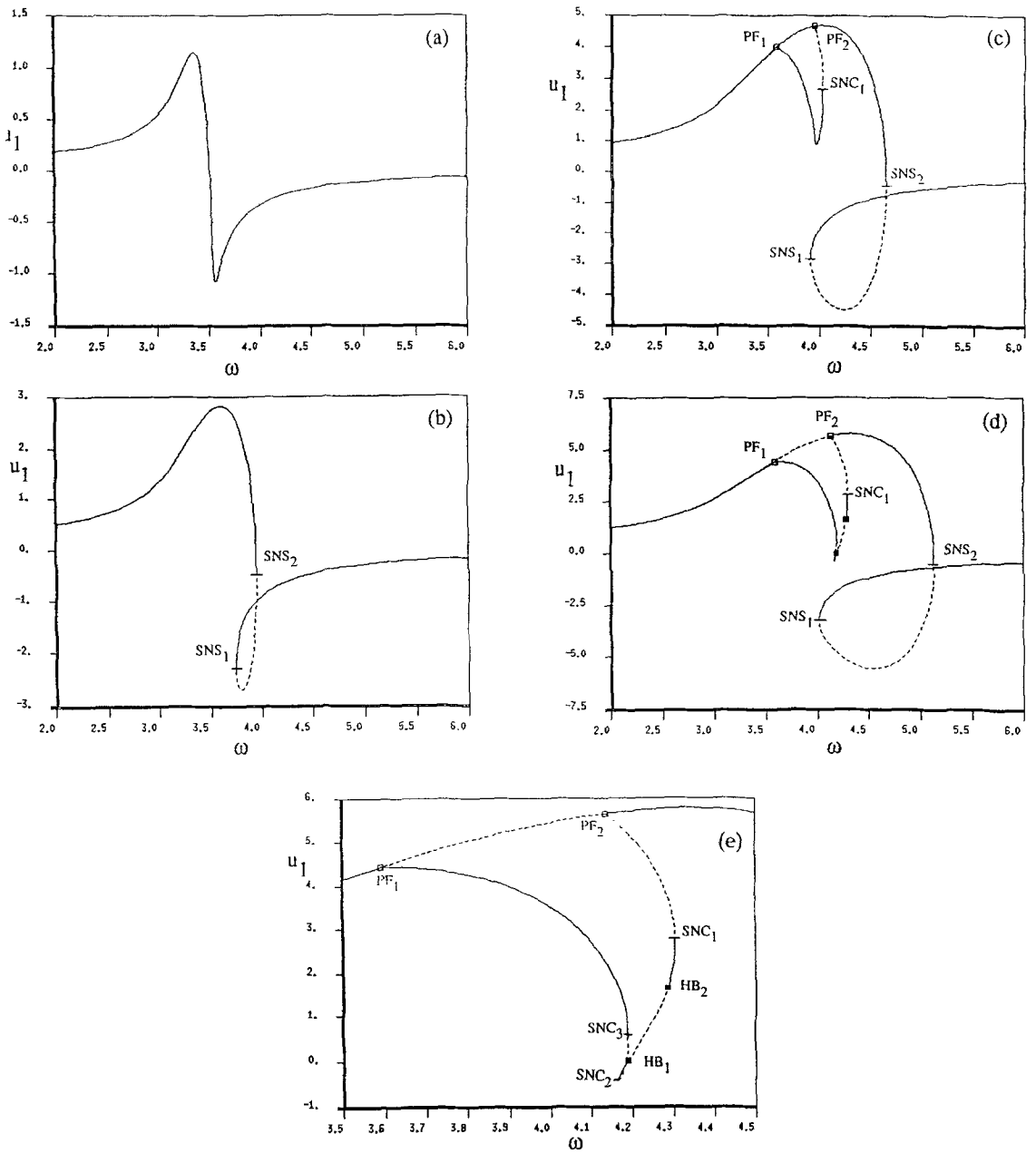

Fig. 6. Bifurcation diagrams at various force levels; $c = 0.195$, $Q_2 = 0.0$. (a) $Q_1 = 1.5$, (b) $Q_1 = 4.0$, (c) $Q_1 = 7.5$, (d) and (e) $Q_1 = 10.0$.

so that two stable coupled-mode motions are possible. One of the coupled-mode solutions then develops Hopf bifurcation points that asymptotically approach the saddle-node bifurcation points SNC_2 and SNC_1 as Q_1 becomes large. One example of such response curves is shown in Figures 6d and e. Over the frequency interval bounded by the two branches of the Hopf bifurcation set, it is expected from the Hopf bifurcation theorem [18] that the amplitude equations will possess limit cycle solutions. These solutions will be explored in some detail in the next section.

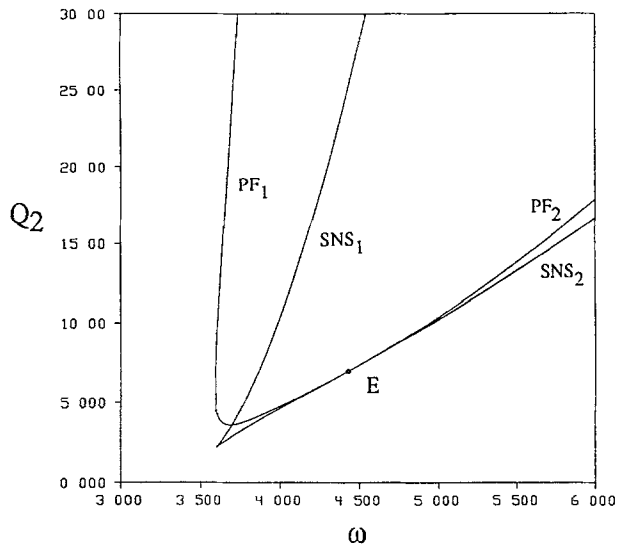

Fig. 7. Saddle-node and pitchfork bifurcation sets for the single-mode solutions; $Q_1 = 0.0$, $c = 0.195$.

A similar stability analysis can be performed for the case of $Q_1 = 0$. Analytical expressions for the results are not given here, but the corresponding bifurcation sets are shown in Figures 7 and 8. The set in Figure 7 is for the single-mode branch, now in the plane defined by (u_2, v_2). Figure 8 gives the bifurcation sets for the coupled-mode motions. There are many qualitatively distinct response diagrams determined by the forcing amplitude Q_2. The most significant difference from the case where the $(1, 2)$ mode is excited occurs in that now there is a codimension-2 point, identified as E in Figures 7 and 8. At this point, the saddle-node, the pitchfork, and the Hopf bifurcation sets meet. In fact the saddle-node and the pitchfork bifurcation sets are tangent without crossing each other. As the forcing amplitude Q_2 is increased this allows for one of the pitchfork points to move from the upper to the middle branch in the single-mode solutions.

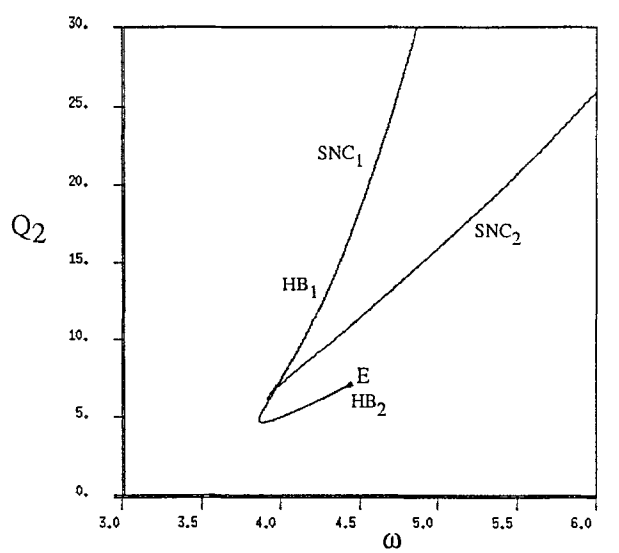

Fig. 8. Saddle-node and Hopf bifurcation sets for the coupled-mode solutions; $Q_1 = 0.0$, $c = 0.195$.

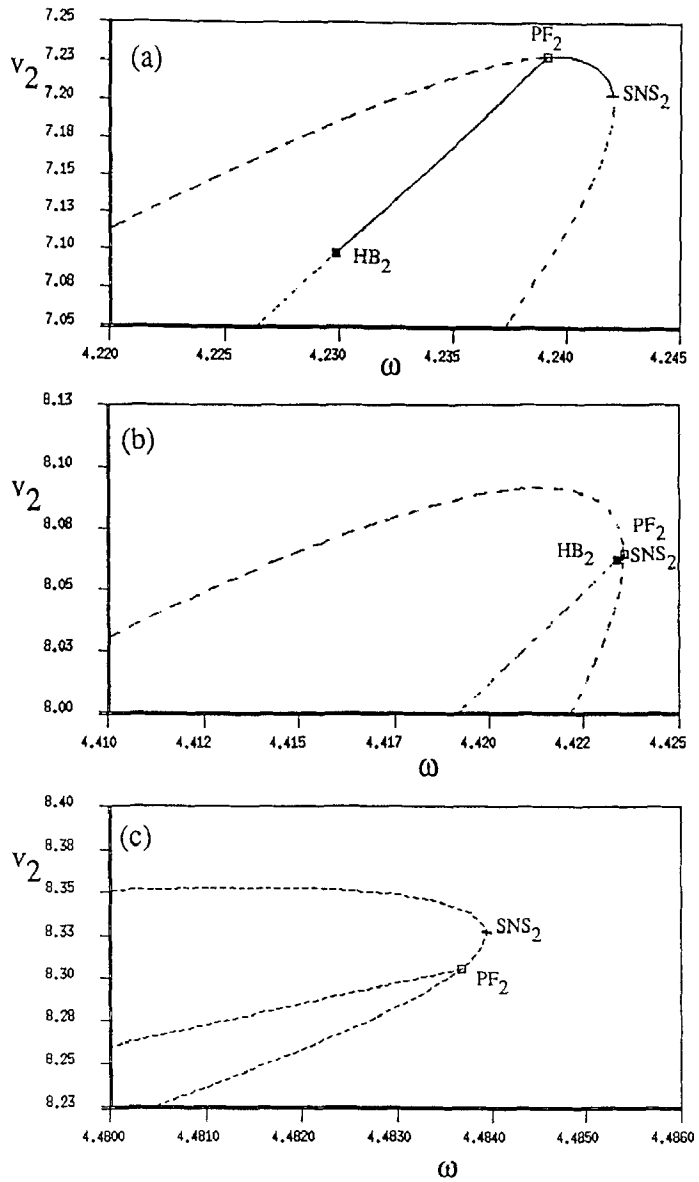

Fig. 9. Evidence of merging at the pitchfork, saddle-node and Hopf bifurcation points; $Q_1 = 0.0$, $c = 0.195$. (a) $Q_2 = 6.0$, (b) $Q_2 = 6.98$, (c) $Q_2 = 7.3$.

Numerical evidence of this behavior is provided in Figure 9 by the amplitude response curves for three close values of Q_2. For $Q_2 = 6.0$ (Figure 9a), the right pitchfork bifurcation point in the single-mode branch is to the left of the turning point with the single-mode solution being stable in the frequency interval ($PF_2 - SNS_2$). The Hopf bifurcation in the coupled-mode branch is at HB_2 and the coupled-mode solution is stable over the frequency interval ($HB_2 - PF_2$). For $Q_2 = 6.98$ (Figure 9b), the three points are nearly coincident, whereas, for $Q_2 = 7.3$, (Figure 9c), all the solutions are unstable and the pitchfork bifurcation takes place in the middle single-mode branch.

In the above discussion, it has been shown for the (1, 2) and (3, 1) interacting modes that for the second case with $Q_1 = 0$, the two pitchfork bifurcation points in the single-mode solutions arise in two different branches. This leads to significant qualitative differences in the response curves

for the two cases and they can be explained easily, for any interacting modes with 1 : 1 internal resonance, by a careful consideration of the equations governing single-mode response and its stability under coupled-mode disturbances. The single-mode motions for $c = 0$ are, in general, solutions of a polynomial of the form (equation (23))

$$R^6 + \frac{8\delta}{3\varepsilon A} R^4 + \frac{16\delta^2}{9\varepsilon^2 A^2} R^2 = \left(\frac{4Q}{3\varepsilon A}\right)^2,$$

which can be factored as

$$\left\{R^2 + \left(\frac{4\delta}{3\varepsilon A}\right) + \frac{4Q}{3\varepsilon AR}\right\}\left\{R^2 + \left(\frac{4\delta}{3\varepsilon A}\right) - \frac{4Q}{3\varepsilon AR}\right\} = 0,$$

where $\delta = \omega^2 - p^2$. The first factor represents the upper branch of single-mode solutions, whereas, the second factor represents the middle and the lower branches. The condition for pitchfork bifurcation (equation (30b)) for the undamped system is of the form

$$\frac{3\varepsilon^2 B^2 R^4}{16} + \varepsilon B\delta R^2 + \delta^2 = 0,$$

where B is the nonlinear coupling coefficient. The two pitchfork points are the roots given by

$$\delta_1 = -\frac{3}{4}\varepsilon BR^2 \quad \text{and} \quad \delta_2 = -\frac{1}{4}\varepsilon BR^2,$$

with $\delta_1 > \delta_2$ for $B < 0$. Using these roots in the expressions for the upper and the lower branches, and requiring that $R^2 > 0$, it is easy to show that δ_2 occurs in the upper branch if $B/A < 3$. Otherwise, this point occurs in the middle branch. Similarly, the point corresponding to δ_1 occurs in the upper branch if $B/A < 1$, otherwise it arises in the middle branch. These conclusions assume that both A and B are negative.

The results derived above allow us to classify all the rectangular plate responses with two interacting modes in 1 : 1 resonance, based on the nonlinear coefficients. Consider, for example, the results of interaction of (1, 2) and (3, 1) modes presented here. In case of $Q_2 = 0$, $A = A_1 = -326.27$ and $B = A_2 = -274.74$, so that $B/A = 0.84 < 1.0$. Thus, both the points corresponding to δ_1 and δ_2 should appear in the upper branch. In case of $Q_1 = 0$, $A = A_3 = -268.32$ and $B = A_2 = -274.74$, so that $B/A = 1.02$. Thus, the point δ_2 should arise in the upper branch and the point δ_1 should arise in the middle branch. The response curves in Figures 2 and 3 are completely consistent with these predictions.

Response curves have also been determined for mode interactions at many other aspect ratios. In particular, Figure 1 shows that (2, 2) and (3, 1) modes are in 1 : 1 resonance for $\kappa \approx 1.291$. The corresponding nonlinear coefficients are calculated to be $A_1 = -500.70$, $A_2 = -664.55$, and $A_3 = -630.52$. The above analysis then predicts that the two pitchfork bifurcation points for both the cases of $Q_2 = 0$ and $Q_1 = 0$ arise in different branches, and these results are found to be completely consistent with the numerically calculated response curves.

Results presented in this section clearly show that, depending on the amplitude and frequency of the external force, the plate can vibrate in various harmonic motions: single-mode, coupled-mode, etc. There also exists the possibility that the amplitude and phase of the response execute limit cycle motions and this is explored in the next section.

4. Periodic and Chaotic Solutions

The numerical study on periodic solutions of the averaged equations has been performed using direct time integration as well as using AUTO [16] a software package which can perform two-parameter bifurcation analysis and continuation for ordinary differential equations. Both the cases of $Q_1 \neq 0$, $Q_2 = 0$ and $Q_1 = 0$, $Q_2 \neq 0$ have been investigated though the results here will be restricted mostly to the former case.

Consider the averaged equations (28) for $Q_2 = 0$. The plane defined by $u_2 = v_2 = 0$ is an invariant manifold and on this submanifold the dynamical behavior is determined by two first-order differential equations governing the variables u_1 and v_1. The divergence of the vector field restricted to the $u_2 = v_2 = 0$ submanifold, $\partial \dot{u}_1/\partial u_1 + \partial \dot{v}_1/\partial v_1$, is $-c$ which is always of the same sign. Thus, for the planar system, Bendixon's criterion [18] is satisfied and limit cycles are ruled out. If there are periodic solutions for the averaged equations, they only arise in the complete 4-dimensional system.

From the bifurcation sets in Figures 4 and 5, it has been seen that so long as the excitation

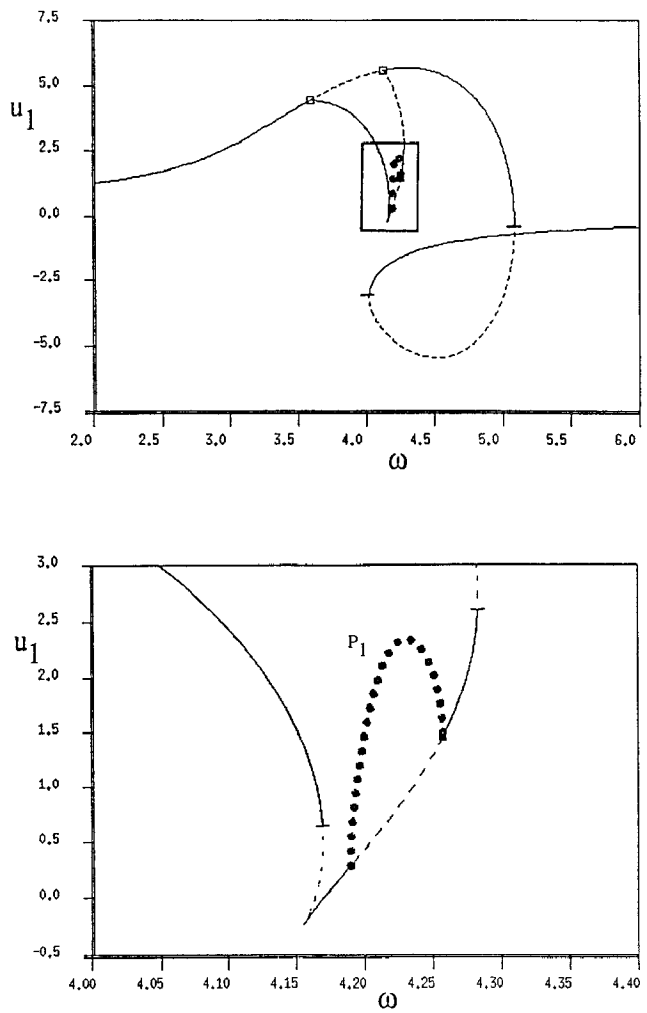

Fig. 10. Response amplitude u_1 as a function of the excitation frequency; $Q_1 = 10.0$, $Q_2 = 0.0$, $c = 0.20$.

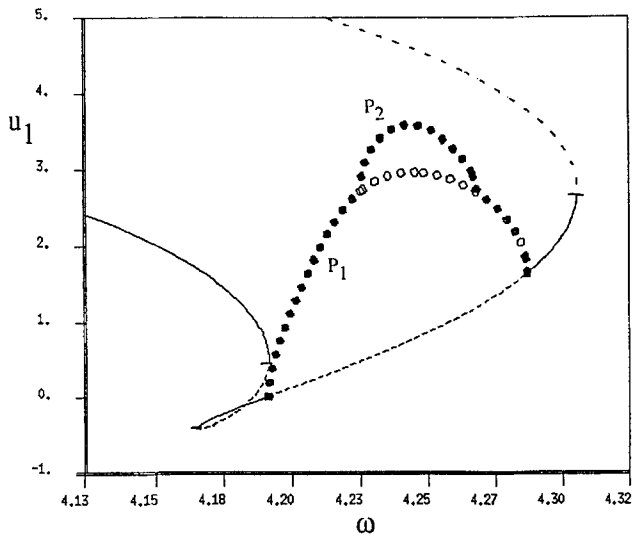

Fig. 11. Response amplitude u_1 as a function of the excitation frequency; $Q_1 = 10.0$, $Q_2 = 0.0$, $c = 0.195$.

force Q_1 is sufficiently low, say, less than Q_1^*, the response is limited to the directly excited (1, 2) mode. For a higher level of the excitation force Q_1, however, the (3, 1) mode also gets excited due to the interaction between the two modes. As the excitation Q_1 increases further, say, above Q_1^{**}, some of the coupled-mode steady-state constant solutions excited through the mechanism of internal resonance lose stability due to a Hopf bifurcation and the averaged system develops periodic solutions from the Hopf bifurcation point. These periodic solutions, denoted as P_1 solutions, correspond to amplitude- and phase-modulated motions of the rectangular plate. The modulated motions result in slow, harmonic oscillations of the nodal pattern. The P_1 solutions branch connects the two Hopf bifurcation points in a coupled-mode steady-state solution branch and is initially (for Q_1 near Q_1^{**}) stable over the frequency interval over which it exists. Figure 10 shows the response curve of steady-state solutions for $Q_1 = 10.0$ and $c = 0.20$ for the amplitude component u_1, as obtained by AUTO. Here the stable limit cycles branch is denoted by small

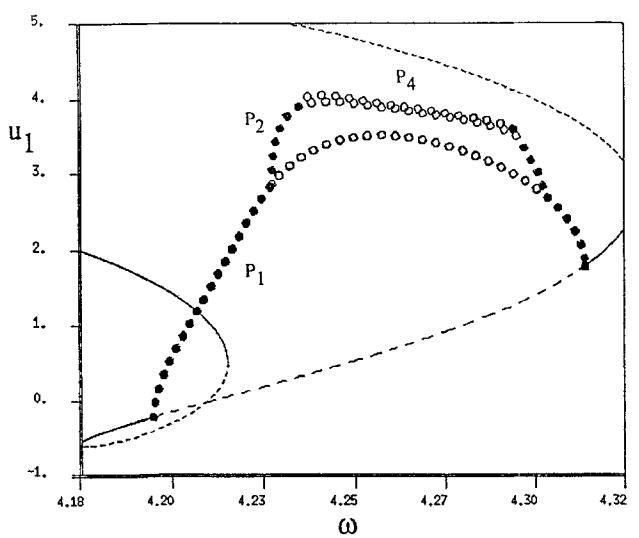

Fig. 12. Response amplitude u_1 as a function of the excitation frequency; $Q_1 = 10.0$, $Q_2 = 0.0$, $c = 0.19$.

solid circles. Both the left and the right Hopf points are supercritical. As the damping is lowered, the P_1 solutions lose stability due to a period-doubling bifurcation. The newly developed branch of periodic solutions with twice the period (denoted as P_2 solutions) connects the two period-doubling bifurcation points in the P_1 solutions branch. (Figure 11; $Q_1 = 10.0$, $c = 0.195$). Here, open circles denote unstable periodic solutions. Decreasing the damping gradually we observe much more complex phenomena including a cascade of period-doubling bifurcations which results in chaotic solutions. We concentrate our discussion on the parameter values $Q_1 = 10.0$, $Q_2 = 0.0$, and $c = 0.19$, for which a portion of the response diagram with periodic solutions is shown in Figure 12. Direct integration of the averaged system with these parameter values for values of excitation frequency ω near the left Hopf bifurcation point $\omega = 4.195$, leads to the steady-state solutions shown in Figure 13. Clearly, the amplitude response at $\omega = 4.237$ is chaotic and results

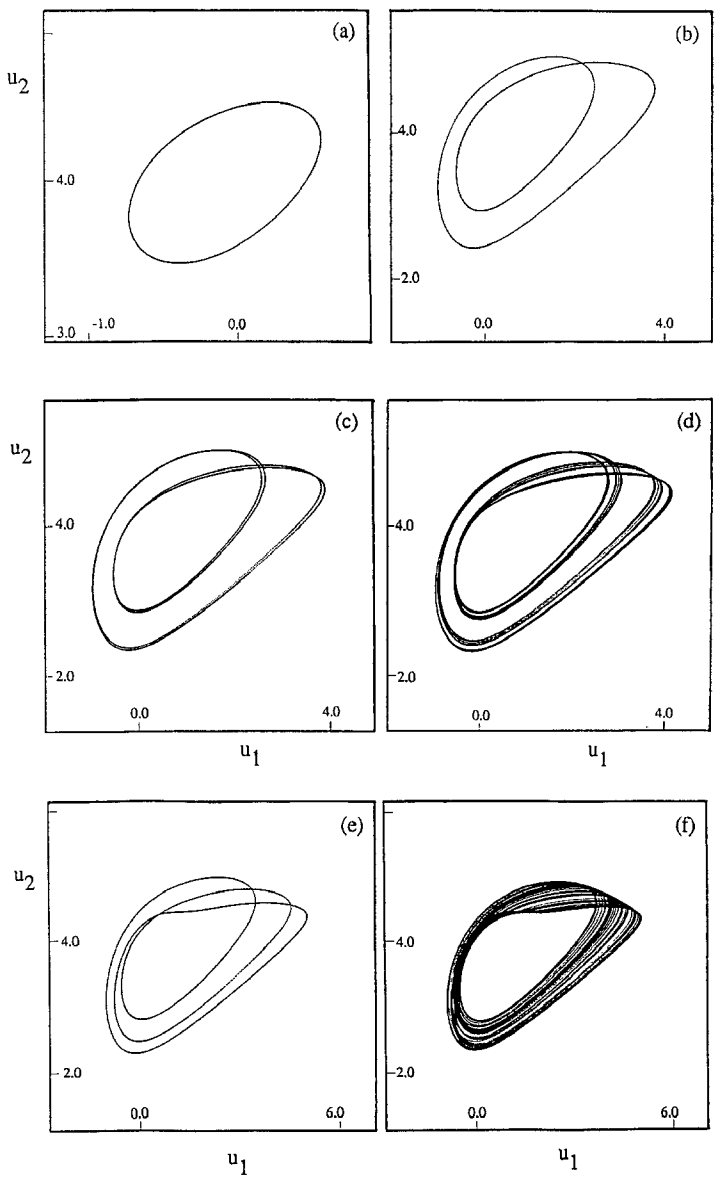

Fig. 13. Phase plots for the steady-state solutions in the Hopf bifurcating branch; $Q_1 = 10.0$, $Q_2 = 0.0$, $c = 0.19$. (a) $\omega = 4.2$ (P_1), (b) $\omega = 4.23$ (P_2), (c) $\omega = 4.235$ (P_4), (d) $\omega = 4.237$ (Ch.), (e) $\omega = 4.2425$ (P_3), (f) $\omega = 4.248$ (Ch.).

from a period-doubling cascade. In the frequency interval with chaotic solutions, there also arise the usual windows of various periods, with the prominent period-3 (P_3) solution at $\omega = 4.2425$ shown in the figure. No stable steady-state solutions in this branch are found beyond $\omega = 4.248$, that is, almost every initial condition for frequencies to the right of $\omega = 4.248$ results in steady-state motions quite distinct from the one at $\omega = 4.248$. A very similar sequence of periodic solutions and period-doubling bifurcations takes place from the right Hopf point ($\omega = 4.313$) in the coupled-mode constant solutions branch. No steady-state motions are found in this branch for $\omega < 4.289$. It is interesting to note that two distinct stable single-mode constant solutions coexist over most of the frequencies where these periodic and chaotic motions are found in the coupled-mode solutions branch. Thus, the plate motions are highly dependent on initial conditions. A Poincaré section of the chaotic solution for $\omega = 4.248$, and with the section taken at $U_2 = 3.0$, is shown in Figure 14.

While numerically investigating the above solutions branch developed from the Hopf bifurcation points, a new and different solutions branch was discovered and the results of direct integration are shown in Figure 15. This branch (henceforth called the "isolated" branch) corresponds to a limit cycle as the primary solution and arises due to a saddle-node bifurcation, that is, a stable and an unstable limit cycle arise at some low enough damping and the branch exists over a small frequency interval. As the damping c is decreased, the stable limit cycle branch undergoes a sequence of period-doubling bifurcations which ultimately lead to chaotic attractors. For $c = 0.19$, the isolated branch arises at $\omega \approx 4.238$, goes through bifurcations and ultimately terminates at $\omega \approx 4.291$, again, via a saddle-node bifurcation. Figure 16 shows qualitatively the relationship between the isolated branch and the branch originating at Hopf points.

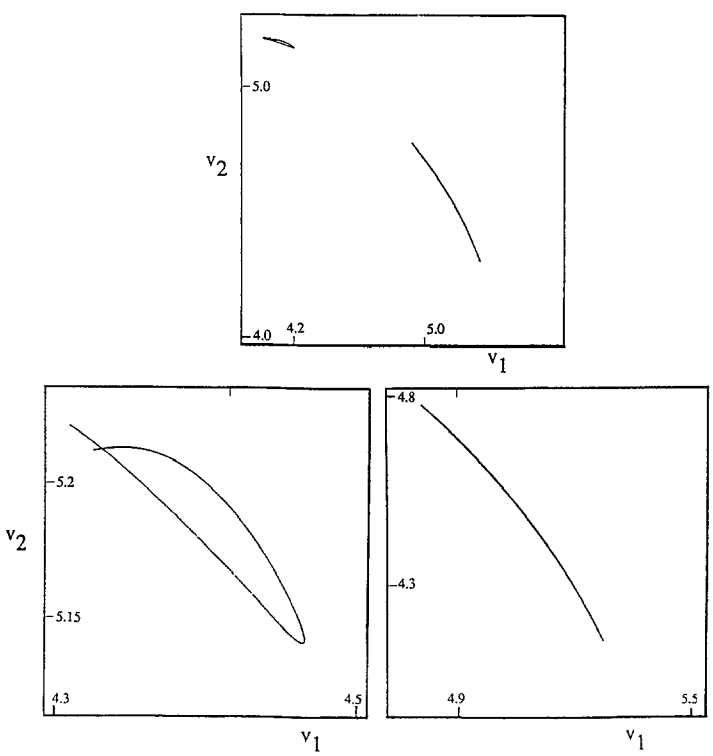

Fig. 14. Projection of the Poincaré section of the chaotic attractor at $\omega = 4.248$; $Q_1 = 10.0$, $c = 0.19$.

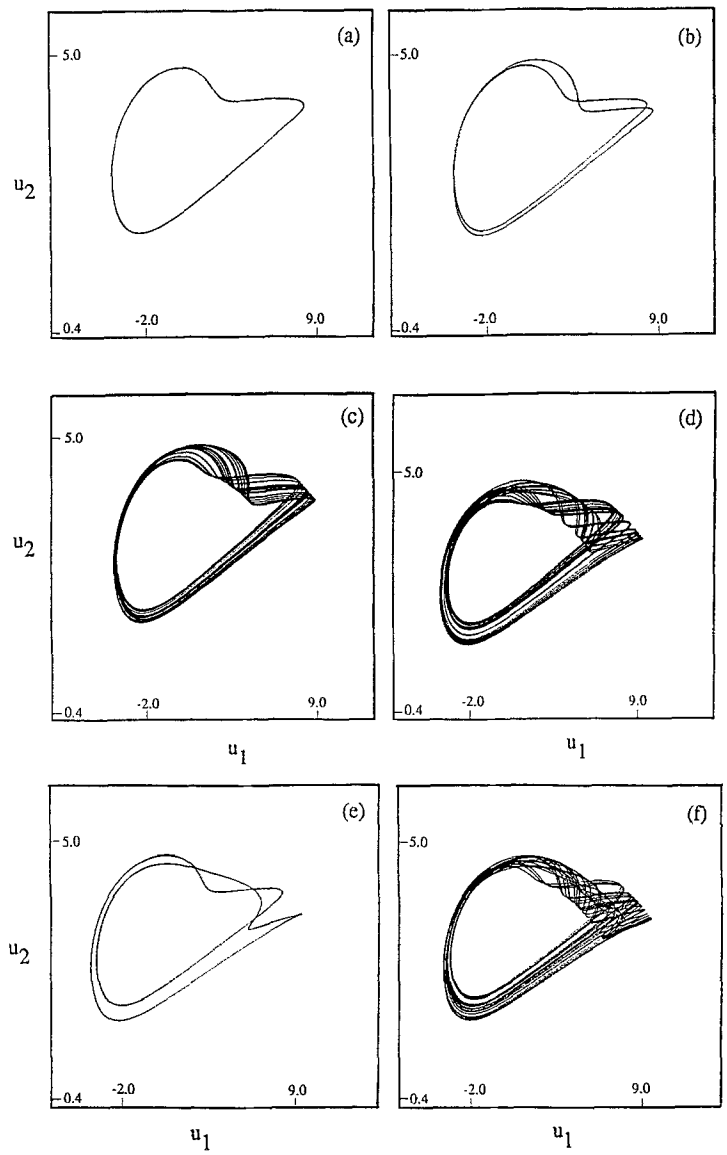

Fig. 15. Phase plots for the steady-state solutions in the isolated branch; $Q_1 = 10.0$, $Q_2 = 0.0$, $c = 0.19$. (a) $\omega = 4.238$ (P_1), (b) $\omega = 4.241$ (P_2), (c) $\omega = 4.243$ (Ch.), (d) $\omega = 4.2485$ (Ch.), (e) $\omega = 4.249$ (P_3), (f) $\omega = 4.255$ (Ch.).

The qualitative behavior conjectured here has since been verified using AUTO [16] where it is also found that the isolated branch itself has a complicated structure. Similar behavior was observed by Bajaj and Johnson [11, 19] in the amplitude dynamics of stretched strings. Figures 13 and 15 clearly show that different periodic and chaotic solutions also coexist with other simpler stable steady-state solutions. In the frequency interval $4.263 \leq \omega \leq 4.268$, Figure 16, no nonconstant steady-state solutions are found for the averaged equations. Almost all initial conditions result in the transients being ultimately captured by the domain of attraction of the single-mode constant steady-state solutions. This can be explained by the concept of a 'crisis' [20], whereby, the chaotic attractor touches the stable manifold of a saddle-type equilibrium point or limit cycle and is destroyed. Figure 17a shows the chaotic attractor at $\omega = 4.262$. The Sil'nikov [21, 22] type

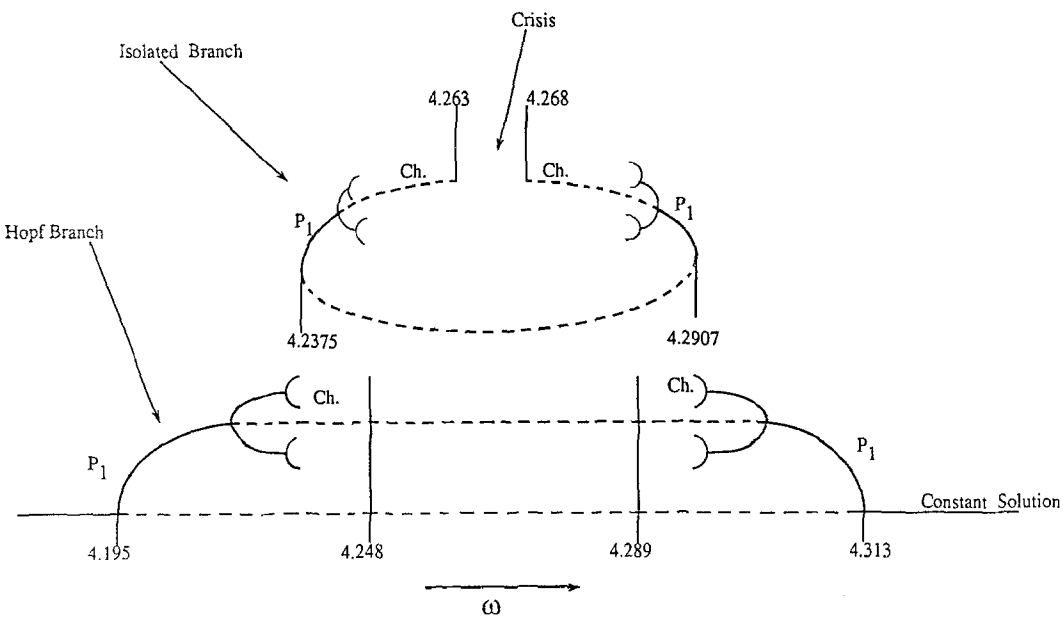

Fig. 16. Qualitative relationship between the Hopf and the isolated solution branches; $Q_1 = 10.0$, $Q_2 = 0.0$, $c = 0.19$.

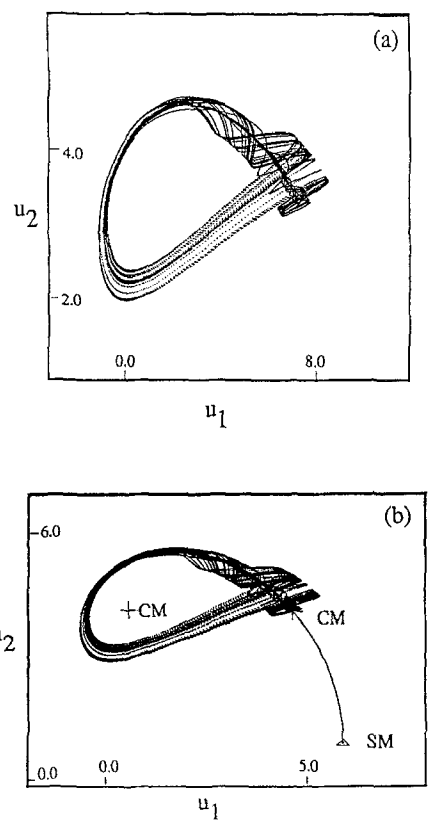

Fig. 17. 'Crisis' in the averaged equations; $Q_1 = 10.0$, $Q_2 = 0.0$, $c = 0.19$. (a) chaotic attractor, $\omega = 4.262$, (b) transient chaos, $\omega = 4.264$.

spiral structure near the right side of the attractor is very evident. This is in the vicinity of the saddle-type coupled-mode constant solution which has a positive real eigenvalue, a negative real eigenvalue and a complex conjugate pair in the left-half plane. Thus, the saddle-point has a one-dimensional unstable manifold and a three-dimensional stable manifold. The chaotic attractor is the closure of the unstable manifold and is enclosed by the stable manifold. For $\omega = 4.264$, Figure 17b shows the transient chaos where the solution traces the ghost of the previous attractor for some time, touches the stable manifold of the saddle-point (CM) and then is quickly attracted by the single-mode constant solution (SM). Figure 18 shows the Poincaré section of the chaotic attractor for $\omega = 2.262$, with the surface defined by $u_2 = 4.0$.

Before closing let us make a few remarks regarding the solutions expected of the discretized two-degrees-of-freedom system represented by equations (19) when the averaged equations possess limit cycle and chaotic solutions. The theorems in method of averaging [14, 18] and the theory of integral manifolds [14] predict that the limit cycle solutions of the amplitude or averaged equations correspond to quasi periodic solutions of equations (19) with two fundamental frequencies. These quasiperiodic motions can be interpreted as motion on a two-torus. Also, for sufficiently small motions characterized by the small parameter of asymptotic analysis, chaotic solutions of the averaged equations are expected to correspond to chaotic amplitude- and phase-modulated solutions of the coupled oscillators. Strong numerical evidence of the ability of asymptotic methods in predicting the complex responses, including chaotic motions and 'crisis', is provided in recent investigations with the string [19, 23]. Since the two oscillators represent

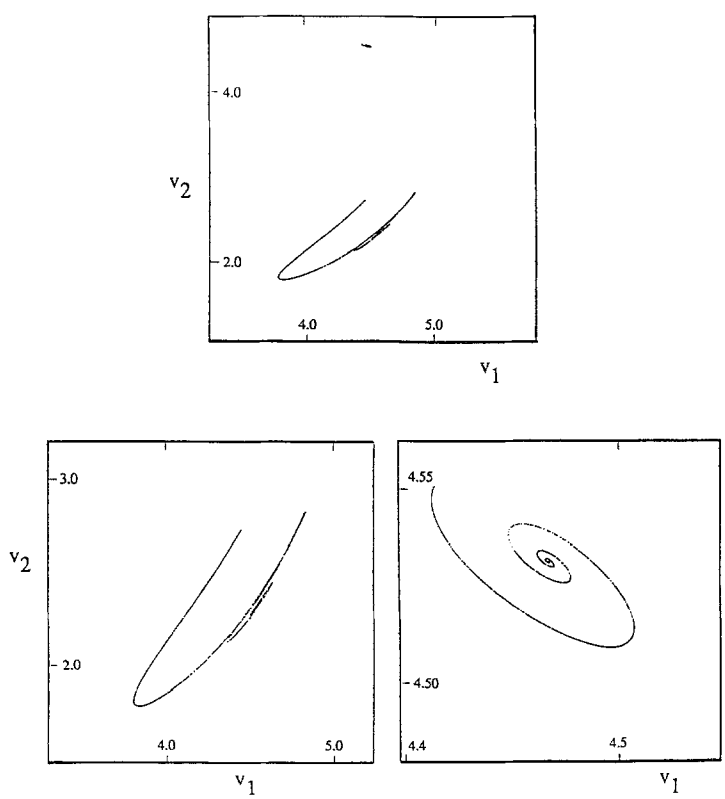

Fig. 18. Projection of the Poincaré section of the chaotic attractor at $\omega = 4.262$; $Q_1 = 10.0$, $c = 0.19$.

amplitudes of the two interacting modes, the plate responds in a chaotically modulated manner in time although the spatial response is simple, consisting of a combination of only two spatial modes.

5. Summary and Conclusions

This work considered the nonlinear vibratory response of a uniformly stretched rectangular plate pinned to immovable supports at its edges. The plate is harmonically excited near primary resonance when two distinct spatial modes are in 1 : 1 internal resonance. The method of averaging is used to investigate the response of the two coupled oscillators representing the dynamics of the two modes in resonance.

Steady-state solutions of the averaged equations are studied in considerable detail. Emphasis is on determining the conditions which lead to coupled-mode response when only one of the modes in resonance is externally excited. It is shown that, depending on the mode combinations in response, as well as the mode that is excited, qualitatively distinct response diagrams can be obtained. Stable single-mode and coupled-mode responses are found to coexist over a wide frequency interval. At low damping levels, the mixed-mode periodic response undergoes Hopf bifurcation to amplitude- and phase-modulated motions. These limit cycles in the averaged equations are found to lead to period-doubling bifurcations to chaotic motions which represent chaotic amplitude- and phase-modulated response of the plate. At lower levels of damping, a 'crisis' can interrupt the chaotic behavior and the plate can unexpectedly jump to small amplitude single-mode harmonic motions as the frequency of excitation is varied.

Acknowledgement

The authors would like to thank Professor P. Davies for a careful reading of the manuscript and for the many useful suggestions. The authors (SIC and AKB) would also like to thank the U.S. Army Research Office for financial support provided under the grant DAAL 03-90-G-0220. Dr. G. L. Anderson is the program monitor.

Appendix

The expressions for the nonlinear coefficients A_1, A_2 and A_3 in equation (19) are given as follows:

$$A_1 = \frac{\pi^4}{16\kappa^4(1-\nu^2)}[(\nu^2-3)(m^4+\kappa^4 n^4) - 4\nu\kappa^2 m^2 n^2],$$

$$A_3 = \frac{\pi^4}{16\kappa^4(1-\nu^2)}[(\nu^2-3)(r^4+\kappa^4 s^4) - 4\nu\kappa^2 r^2 s^2],$$

$$A_2 = -\frac{\pi^4}{8\kappa^4(1-\nu)^2}[m^2r^2 + \nu\kappa^2(r^2n^2+s^2m^2) + \kappa^4 s^2 n^2]$$
$$+ \frac{1}{[(m-r)^2+\kappa^2(n-s)^2]^2}\left[-\frac{\pi^4}{16}(nr-ms)^4 - \frac{B}{(m^2-r^2)(n^2-s^2)}\right]$$

$$+\frac{1}{[(m+r)^2+\kappa^2(n-s)^2]^2}\left[-\frac{\pi^4}{16}(nr+ms)^4-\frac{B_2}{(m^2-r^2)(n^2-s^2)}\right]$$
$$+\frac{1}{[(m-r)^2+\kappa^2(n+s)^2]^2}\left[-\frac{\pi^4}{16}(nr+ms)^4-\frac{B_3}{(m^2-r^2)(n^2-s^2)}\right]$$
$$+\frac{1}{[(m+r)^2+\kappa^2(n+s)^2]^2}\left[-\frac{\pi^4}{16}(nr-ms)^4-\frac{B_4}{(m^2-r^2)(n^2-s^2)}\right]$$
$$+\frac{B_5}{\kappa^2(1+\nu)(m^2-r^2)^2(n^2-s^2)^2},$$

where $B_i=0$, $i=1, 2, 3, 4, 5$ for $N_{xy0}=0$, and

$$B_1=32mnrs(nr-ms)^2,$$
$$B_2=-32mnrs(nr+ms)^2,$$
$$B_3=-32mnrs(nr+ms)^2,$$
$$B_4=32mnrs(nr-ms)^2,$$
$$B_5=128m^2n^2r^2s^2$$
for $N_{xy0}\neq 0$.

The expressions for coefficients C_i, $i=1, 2, 3, 4, 5$ in equation (15) depend on the solutions $\hat{R}_1$ in equation (25), and are given as follows:

(a) For $+ve$ sign in equation (25):

$$C_1=\frac{9}{64}\frac{\varepsilon^2A_3^2(A_2^2-9A_1A_3)^2}{\omega^2A_2^4},$$
$$C_2=\frac{3}{8}\frac{\varepsilon A_3(A_2^2-9A_1A_3)}{\omega^2A_2^4}[3A_2A_3\sigma_1+(A_2^2-18A_1A_3)\sigma_2],$$
$$C_3=\frac{1}{4A_2^2\omega^2}[9A_2^2A_3^2\sigma_1^2+6A_2A_3(2A_2^2-27A_1A_3)\sigma_1\sigma_2+(A_2^4-54A_1A_2^2A_3+486A_1^2A_3^2)\sigma_2^2],$$
$$C_4=\frac{3}{4}\frac{A_3}{A_2}\frac{Q_1^2}{\omega^2}+\frac{2\sigma_2}{\varepsilon\omega^2A_2^4}[3A_2^2A_3\sigma_1^2+A_2(A_2^2-27A_1A_3)\sigma_1\sigma_2-3A_1(A_2^2-18A_1A_3)\sigma_2^2],$$
$$C_5=\frac{4\sigma_2}{\varepsilon A_2}\left[\frac{Q_1^2}{4\omega^2}+\frac{\sigma_2}{\varepsilon A_2^3\omega^2}(A_2\sigma_1-3A_1\sigma_2)^2\right],$$

where $\sigma_1=\omega^2-p_1^2$ and $\sigma_2=\omega^2-p_2^2$.

(b) For $-ve$ sign in equation (25):

$$C_1=\frac{9}{64}\frac{\varepsilon^2A_3^2(A_2^2-A_1A_3)^2}{\omega^2A_2^4},$$
$$C_2=\frac{3}{8}\frac{\varepsilon A_3(A_2^2-A_1A_3)}{\omega^2A_2^4}[A_2A_3\sigma_1+(A_2^2-2A_1A_3)\sigma_2],$$

$$C_3 = \frac{1}{4A_2^2\omega^2}[A_2^2A_3^2\sigma_1^2 + 2A_2A_3(2A_2^2 - 3A_1A_3)\sigma_1\sigma_2 + (A_2^4 - 6A_1A_2^2A_3 + 6A_1^2A_3^2)\sigma_2^2],$$

$$C_4 = \frac{1}{4}\frac{A_3}{A_2}\frac{Q_1^2}{\omega^2} + \frac{2\sigma_2}{3\varepsilon\omega^2A_2^4}[A_2^2A_3\sigma_1^2 + A_2(A_2^2 - 3A_1A_3)\sigma_1\sigma_2 - 3A_1(A_2^2 - 2A_1A_3)\sigma_2^2],$$

$$C_5 = \frac{4\sigma^2}{3\varepsilon A_2}\left[\frac{Q_1^2}{4\omega^2} + \frac{\sigma_2}{3\varepsilon A_2^3\omega^2}(A_2\sigma_1 - A_1\sigma_2)^2\right].$$

References

1 Nayfeh, A. H. and Mook, D. T., *Nonlinear Oscillations*, Wiley-Interscience, New York, 1979.
2. Sathyamoorthy, M., 'Nonlinear vibration of plates – a review', *The Shock and Vibration Digest* **15**, 1983, 3–16.
3. Sathyamoorthy, M., 'Nonlinear vibration analysis of plates: A review and survey of current developments', *Applied Mechanics Review* **40**, 1987, 1553–1561.
4. Miles, J. W., 'Resonant motions of a spherical pendulum', *Physica D* **11**, 1984, 309–323.
5. Tousi, S. and Bajaj, A. K., 'Period-doubling bifurcations and modulated motions in forced mechanical systems', *ASME Journal of Applied Mechanics* **107**, 1985, 446–452.
6. Miles, J. W., 'Resonantly forced motion of two quadratically coupled oscillators', *Physica D* **13**, 1984, 247–260.
7. Nayfeh, A. H. and Balachandran, B., 'Modal interactions in dynamical and structural systems', *Applied Mechanics Review* **42**, 1989, S175–S201.
8. Sridhar, S., Mook, D. T., and Nayfeh, A. H., 'Nonlinear resonances in the forced responses of plates, Part II: Asymmetric responses of circular plates', *Journal of Sound and Vibration* **59**, 1978, 159–170.
9. Maewal, A., 'Chaos in a harmonically excited elastic beam', *ASME Journal of Applied Mechanics* **53**, 1986, 625–632.
10. Yasuda, K. and Torii, T., 'Multi-mode response of a square membrane', *JSME International Journal* **30**, 1987, 963–969.
11. Johnson, J. M. and Bajaj, A. K., 'Amplitude modulated and chaotic dynamics in resonant motion of strings', *Journal of Sound and Vibration* **128**, 1989, 87–107.
12. Yang, X. L. and Sethna, P. R., 'Nonlinear phenomena in forced vibrations of a nearly square plate – antisymmetric case', *Journal of Sound and Vibration* 155, 1992, 413–441.
13. Yasuda, K. and Asano, T., 'Nonlinear forced oscillations of a rectangular membrane with degenerate modes', *Bulletin of JSME* **29**, 1986, 3090–3095.
14. Hale, J. K., *Ordinary Differential Equations*, Wiley-Interscience, New York, 1969.
15. Maewal, A., 'Miles' evolution equations for axisymmetric shells: Simple strange attractors in structural dynamics', *International Journal of Non-linear Mechanics* **21**, 1987, 433–438.
16. Doedel, E., *AUTO: Software for continuation and bifurcation problems in ordinary differential equations*, Report, Department of Applied Mathematics, California Institute of Technology, 1986.
17. Pai, P. F. and Nayfeh, A. H., 'A nonlinear composite plate theory', *Nonlinear Dynamics* **2**, 1991, 445–477.
18. Guckenheimer, J. and Holmes, P. J., *Nonlinear Oscillations, Dynamical Systems and Bifurcations of Vector Fields*, Springer-Verlag, New York, 1983.
19. Bajaj, A. K. and Johnson, J. M., 'On the amplitude dynamics and 'crisis' in resonant motion of stretched strings', *Philosophical Transactions of the Royal Society London* **A338**, 1992, 1–41.
20. Grebogi, C., Ott, E., and Yorke, J. A., 'Crises, sudden changes in chaotic attractors, and transient chaos', *Physica D* **7**, 1983, 181–200.
21. Sil'nikov, L. P., 'A contribution to the problem of the structure of an extended neighborhood of a rough equilibrium state of saddle-focus type', *Mathematics USSR Sbornik* **10**, 1970, 91–102.
22. Glendenning, P. and Sparrow, C., 'Local and global behavior near homoclinic orbits', *Journal of Statistical Physics* **35**, 1984, 645–696.
23. Bajaj, A. K. and Johnson, J. M., 'Asymptotic techniques and complex dynamics in weakly non-linear forced mechanical systems', *International Journal of Non-Linear Mechanics* **25**, 1990, 211–226.